Abdominal Radiology (2019) 44:992–999
https://doi.org/10.1007/s00261-018-01889-x

PANCREAS

Differentiation of pancreatic neuroendocrine tumors from pancreas renal cell carcinoma metastases on CT using qualitative and quantitative features

Christian B. van der Pol[1] · Stefanie Lee[1] · Scott Tsai[1] · Natasha Larocque[1] · Abdullah Alayed[2] · Phillip Williams[3] · Nicola Schieda[2]

Published online: 2 January 2019

Abstract

Purpose To assess qualitative and quantitative imaging features on enhanced CT that may differentiate pancreatic neuroendocrine tumors (PNETs) from pancreatic renal cell carcinoma (RCC) metastases.

Methods This IRB-approved multi-center retrospective case–control study compared 43 resected PNETs and 28 resected RCC metastases with pre-operative enhanced CT identified consecutively between 2003 and 2017. Two blinded radiologists (R1/R2) independently assessed tumor location, attenuation (relative to pancreas), composition (solid/cystic/mixed), homogeneity (homogeneous/heterogeneous), calcification, multiplicity, and for main pancreatic duct (MPD) dilation. Tumors were segmented for quantitative texture analysis. Data were analyzed with Chi square, logistic regression, and receiver operating characteristic (ROC). Inter-observer agreement was assessed (Cohen's kappa).

Results There was no difference in age, gender, location, attenuation, or composition ($P > 0.05$) between groups. PNETs were larger than RCC metastases (37 ± 23 mm vs. 26 ± 21 mm, $P = 0.038$), more frequently solitary ($P < 0.001$), subjectively more heterogeneous ($P = 0.033/0.144$, R1/R2), and associated with calcification ($P = 0.002/0.004$) and MPD dilation ($P = 0.025/0.006$). Agreement for subjective features was moderate-to-almost perfect ($K = 0.4879$–0.9481). Quantitative texture analysis showed higher entropy in PNETs (6.32 ± 0.49 versus 5.96 ± 0.53; $P = 0.004$) with no difference in other features studied ($P > 0.05$). Entropy had ROC area under the curve for diagnosis of PNET of 0.77 ± 0.06, with optimal sensitivity/specificity of 71.4/79.1%.

Conclusions Compared to pancreatic RCC metastases, PNETs are larger, more frequently solitary, contain calcification, show MPD dilation, and are subjectively and quantitatively more heterogeneous tumors.

Keywords Pancreatic neuroendocrine tumor · Renal cell carcinoma · Pancreas · X-ray computed tomography

✉ Christian B. van der Pol
vanderpolc@hhsc.ca

Stefanie Lee
leestef@hhsc.ca

Scott Tsai
tsai@hhsc.ca

Natasha Larocque
natasha.larocque@medportal.ca

Abdullah Alayed
alayed18@gmail.com

Phillip Williams
williamsph@hhsc.ca

Nicola Schieda
nschieda@toh.on.ca

[1] Department of Diagnostic Imaging, Juravinski Hospital and Cancer Centre, Hamilton Health Sciences, McMaster University, 711 Concession Street, Hamilton, ON L8V 1C3, Canada

[2] Department of Diagnostic Imaging, The Ottawa Hospital- Civic Campus, 1053 Carling Avenue, Ottawa, ON K1Y 4E9, Canada

[3] Department of Pathology and Molecular Medicine, Juravinski Hospital and Cancer Centre, Hamilton Health Sciences, McMaster University, 711 Concession Street, Rm F1-103, Hamilton, ON L8V 1C3, Canada

Abbreviations

CECT	Contrast-enhanced CT
DICOM	Digital imaging and communications in medicine
EUS	Endoscopic ultrasound
FNA	Fine needle aspiration
JMRI	Journal of Magnetic Resonance Imaging
MPD	Main pancreatic duct
PNET	Pancreatic neuroendocrine tumor
RCC	Renal cell carcinoma
ROI	Region of interest

Introduction

Renal cell carcinoma (RCC) is among the most common primary malignancies that metastasize to the pancreas and typically appears as a hypervascular pancreatic mass on CT or MRI [1–3]. RCC metastases can resemble primary pancreatic neuroendocrine tumors (PNETs), which are also commonly hypervascular masses [4]. Both tumors may present in patients with multiple pancreatic masses and both may occur at increased frequency in patients with a variety of genetic syndromes, including Von Hippel–Lindau disease [5]. Up to 10% of patients with metastatic RCC develop pancreatic metastases [6]. Further complicating the differentiation of pancreatic RCC metastases from PNETs is that the pancreas may be the sole site of RCC metastases and pancreatic metastases not uncommonly present as solitary masses many years after treatment of the primary tumor [7, 8].

The management for PNETs and pancreatic RCC metastases differs. Although surgery is generally recommended for treatment of PNETs and especially poorly differentiated PNETs (grade 3) [9], non-functional small (< 2 cm) and well-differentiated PNETs (grade 1 or 2) are sometimes followed on serial imaging given the morbidity of a pancreatectomy [10, 11], while targeted immunotherapy and other systemic treatments can be considered for advanced well-differentiated PNETS [12]. Pancreatic RCC metastases are usually resected if at all possible or, more recently, in non-surgical candidates can be treated with targeted biologic agents [13, 14] and stereotactic body radiotherapy.

The accurate differentiation between PNETs and pancreatic RCC metastases using imaging could preclude the need for histologic sampling to confirm diagnosis and expedite treatment. Histological sampling is required before the initiation of definitive therapy and is performed using endoscopic ultrasound-guided fine needle aspiration (EUS-FNA) which is invasive and may not lead to a diagnosis in pancreatic masses including in up to 21% of PNETs [15, 16]. Furthermore, the morphology of PNETs and pancreatic RCC metastases can overlap on EUS [17]. Recently, CT texture analysis has emerged as a quantitative imaging technique that can help distinguish between various types of neoplasms in the body, tumor mutation status, grade, and prognosis [18–23]; specifically, Canellas et al. showed that among PNETs texture analysis could discriminate between low- and high-grade tumors [23]. The purpose of this study was to compare qualitative and quantitative imaging features on enhanced CT among PNETs and pancreatic RCC metastases.

Materials and methods

This multi-center retrospective case–control study was approved by the respective local Institutional Review Boards, who granted a data-sharing agreement to perform analyses. The requirement for informed consent was waived.

Study cohort

Between January 1, 2011 and October 16, 2017, 70 consecutive patients with resected PNETs and 13 with pancreatic RCC metastases were identified at Hamilton Health Sciences. Pre-operative enhanced CT was not available for 26 patients, two patients had PNETs indistinct from large serous cystadenomas, and one had a pancreas tail PNET invading and indistinct from adjacent infarcted splenic parenchyma, which were excluded, leaving 41 patients with 43 PNETs. Four patients with pancreatic RCC metastases were excluded due to no available pre-operative enhanced CT, leaving nine patients with 11 pancreatic RCC metastases. Medical records at The Ottawa Hospital were then reviewed to augment the number of pancreatic RCC metastases, which identified an additional 21 consecutive patients with pancreatic RCC metastases between November 25, 2003 and October 16, 2017. Of these, 11 patients were excluded as enhanced CT was not available. This yielded the study cohort which consisted of 60 patients (33 males, 27 females, mean age 57.8 years); 41 patients with 43 PNETS and 19 patients with 28 pancreatic RCC metastases (Fig. 1). All RCC metastases were of the clear cell subtype. Of the PNETs, 30 were grade 1, nine were grade 2, and four were grade 3. Mean time from CT to surgery was 117 ± 76 days. The sample was one of convenience which attempted to maximize the number of confirmed PNETs and RCC metastases with pre-operative imaging.

Histopathology

Pathology at surgical resection was used as a reference standard for all PNETs and pancreatic RCC metastases. PNETs were characterized by neuroendocrine features with solid, trabecular, and nested growth patterns, and salt and pepper nuclei. Pancreatic clear cell RCC metastases were characterized by distinctive clear to eosinophilic cytoplasm,

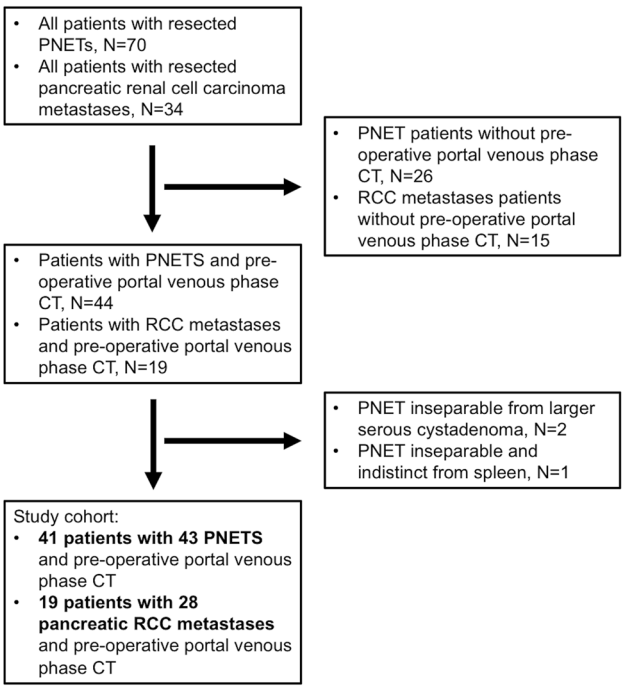

Fig. 1 Patient flow diagram. *PNET* pancreatic neuroendocrine tumor, *RCC* renal cell carcinoma

with a delicate vascular network and frequent hemorrhage. If there was histological uncertainty, immunohistochemistry was performed to confirm the diagnosis, with PNET being positive for cytoplasmic chromogranin and synaptophysin, and negative for monoclonal nuclear PAX8, while clear cell RCC metastases show the reverse immunohistochemistry pattern [24, 25].

CT technique

All patients included in the study had undergone at least one single-phase enhanced CT of the abdomen before surgery. The CT protocols varied but timing of acquisition was in the portal venous phase (timed empirically at approximately 70 s post contrast administration). Minor differences in timing of the portal venous phase were not considered significant. Every examination included axial images of the abdomen (slice thickness 2.5–5 mm) with coronal reconstructed images (slice thickness 3 mm).

Four patients underwent CT on a 320-channel MDCT (Toshiba Aquilion ONE), nine patients on a 256-channel MDCT (GE Revolution CT, Philips iCT 256, Siemens SOMATOM Definition FLASH), eight patients on a 128-channel MDCT (Siemens Definition Edge and AS+), 30 patients using 64-channel MDCT (GE Discovery CT750HD/LightSpeed VCT, Philips Brilliance 64, Siemens Sensation 64, Toshiba Aquilion), and nine patients using 16-channel MDCT (GE LightSpeed Xtra/Plus, Philips Brilliance 16P, Siemens Emotion 16).

Our institutional CT protocols consist of a fixed 120-kVp technique with automated tube current modulation and a variable 100–500-mAs. Acquisition is helical with a rotation time of 0.8 s and a Noise Index of either 31 or 41.4. The timing of the portal venous phase is established empirically in all cases timed to be 65–70 s after the injection of contrast. Patients were given 100–150 mL of non-ionic contrast material (either Iohexol [Omnipaque], GE Healthcare or Iopamidol [Isovue], Bracco Healthcare) at a fixed intravenous rate of 3.0–3.5 mL/s using a power injector followed by a saline flush.

Qualitative image analysis

Two fellowship-trained abdominal radiologists (ST and SL) with 16 and four post-fellowship years of experience, blinded to all clinical information including histopathology findings, independently assessed for tumor location (uncinate process, head, neck, body, or tail), attenuation (hyperdense, isodense, or hypodense compared to adjacent pancreatic parenchyma), composition (totally solid, solid with some cystic areas, cystic with some solid components, cystic) [23], homogeneity (homogeneous [uniform in attenuation] or heterogeneous [mixed areas of attenuation]), calcification (present or absent), multiplicity (one or more than one tumor), and for main pancreatic duct (MPD) dilation (present or absent).

Quantitative image analysis

A fellowship-trained abdominal radiologist (CVP) selected the axial image showing the largest tumor diameter, recorded maximum tumor diameter, and exported the same image in DICOM format from PACS to an independent workstation after patient-identifying information was removed. Tumors were then manually contoured to obtain a region of interest (ROI) that encompassed as much of the tumor as possible while carefully avoiding extra-tumoral structures (Fig. 2). A minimum area of 10 mm^2 was required to obtain accurate measurements as described previously [26]. Using the same axial image where ROI measurements were performed, texture analysis was performed. First-order texture features were extracted by histogram analysis, specifically; *Kurtosis* (a measure of histogram flatness), *Skewness* (a measure of histogram asymmetry), and *Entropy* (a measure of histogram irregularity) as described previously [27]. Manual contouring of tumors was independently repeated in 17% of patients (10/60) for 17 tumors by a second fellowship-trained abdominal radiologist (NS), to assess reproducibility of segmentation (personal communication with Dr. M.E. Schweitzer,

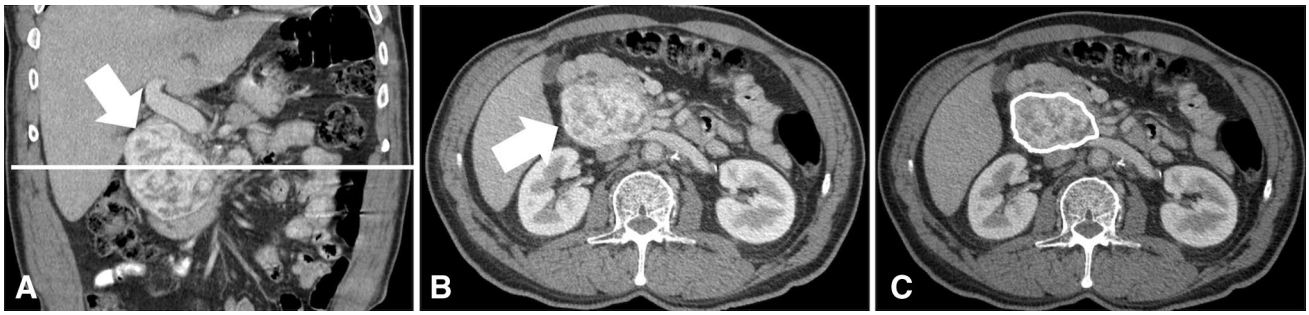

Fig. 2 A 62-year-old male with grade 2 pancreatic neuroendocrine tumor (PNET) in the pancreas head diagnosed after a partial pancreaticoduodenectomy. **a** Coronal contrast-enhanced CT (CECT) image illustrates the tumor (thick white arrow). The horizontal white line corresponds to the axial image that demonstrated the largest diameter of the pancreas head mass. In this way, the axial image where the tumor appeared the largest was used for quantitative assessment. **b** Axial CECT image at the level demarcated in **a**. depicts the tumor (thick white arrow) as a heterogeneous hyperenhancing (relative to the pancreas) mass. **c** Axial CECT image at the same level as **b**. shows methodology for quantitative analysis. A region of interest (ROI) was manually drawn by an Abdominal Radiologist (white outline) for tumor segmentation and texture analysis

Editor-In-Chief JMRI). Lesion analysis was performed using Image J (version 1.48, National Institutes of Health) [28].

Statistical analysis

Mean ± standard deviation with range is reported for quantitative data. Demographic and subjective variables were compared using the Chi-square test of proportions, and quantitative data were compared using multivariable logistic regression analysis. Inter-observer agreement for subjective variables was calculated using Cohen's kappa statistic where 0–0.2 was slight agreement, 0.21–0.4 was fair agreement, 0.41–0.6 was moderate agreement, 0.61–0.80 was substantial agreement, and > 0.81 was almost perfect agreement. Receiver operator characteristic (ROC) curve analysis was performed for statistically significant quantitative variables and diagnostic accuracy calculated for statistically significant subjective data. Reproducibility of segmentation was compared between radiologists using Cohen's kappa statistic and Bland–Altman analysis. Threshold P value < 0.05 indicated a statistically significant difference. Statistical analysis was performed with STATA Data analysis and statistical software, version 13 (Foster City Station, Texas, USA).

Results

A summary of subjective variables assessed by two radiologists is provided in Table 1. Among subjective variables studied, there was no difference in location, attenuation, or composition of PNETs compared to pancreatic RCC metastases for either Radiologist ($P > 0.05$). PNETs were more likely to show calcification ($P = 0.002$ Radiologist 1, 0.004 Radiologist 2) and main pancreatic duct dilation ($P = 0.025$ Radiologist 1, 0.006 Radiologist 2), whereas RCC metastases were more frequently multiple ($P < 0.001$ Radiologist 1 and 2). Pancreatic RCC metastases were more likely to appear homogeneous though the difference was only significant for Radiologist 2 ($P = 0.114$ for Radiologist 1 and 0.033 for Radiologist 2) (Fig. 3). Inter-observer agreement was moderate-to-almost perfect for subjective features evaluated by the Radiologists ($K = 0.4879$–0.9481). Age and gender were not association with tumor type ($P = 0.068$ and 0.802, respectively).

A summary of quantitative variables comparing PNET and pancreatic RCC metastases is provided in Table 2. PNETs were larger than RCC metastases ($P = 0.038$) with no difference in mean or median attenuation between groups ($P = 0.969$ and 0.895 respectively). With respect to texture analysis features studied, entropy was significantly higher in PNETs compared to RCC metastases (6.32 ± 0.49 vs. 5.96 ± 0.53, $P = 0.004$) with a trend towards higher levels of kurtosis and skewness, although the difference in the latter two features did not reach statistical significance between groups ($P = 0.067$ and 0.099, respectively).

A logistic regression model combining size and texture features resulted in an area under the receiver operator characteristic curve of 0.77 (± 0.06) with optimal sensitivity and specificity for diagnosis of PNET of 71.4% and 79.1%, respectively, Fig. 4. Inter-observer agreement for texture analysis measurements was substantial with a low mean difference of 0.21 ± 0.30 (Fig. 5).

Discussion

This study evaluated enhanced CT to differentiate between PNETs and pancreatic RCC metastases. The imaging distinction between these two diagnoses is important because both may present as hypervascular pancreatic masses,

Table 1 Comparison of subjective variables assess by two radiologists in pancreatic neuroendocrine tumors and pancreatic renal cell carcinoma metastases

	Radiologist 1		Radiologist 2		*P* value	Kappa
	PNET *N* = 43	ccRCC metastases *N* = 28	PNET *N* = 43	ccRCC metastases *N* = 28		
Location					*P* = 0.068 (R1)	0.7565
Uncinate process	2 (5%)	1 (4%)	5 (12%)	3 (11%)	*P* = 0.563 (R2)	
Head	13 (30%)	9 (32%)	11 (26%)	7 (25%)		
Neck	7 (16%)	1 (4%)	6 (14%)	2 (7%)		
Body	11 (26%)	15 (54%)	11 (26%)	12 (43%)		
Tail	10 (23%)	2 (7%)	10 (23%)	4 (14%)		
Attenuation					*P* = 0.654 (R1)	0.4879
Hyperattenuating	32 (74%)	19 (68%)	34 (79%)	24 (86%)	*P* = 0.674 (R2)	
Isoattenuating	7 (16%)	7 (25%)	6 (14%)	2 (7%)		
Hypoattenuating	4 (9%)	2 (7%)	3 (7%)	2 (7%)		
Composition					*P* = 0.147 (R1)	0.7201
Completely solid	29 (67%)	25 (89%)	29 (67%)	23 (82%)	*P* = 0.378 (R2)	
Mostly solid, part cystic	9 (21%)	3 (11%)	12 (28%)	4 (14%)		
Mostly cystic, part solid	4 (9%)	0 (0%)	2 (5%)	1 (4%)		
Completely cystic	1 (2%)	0 (0%)	0 (0%)	0 (0%)		
Enhancement					*P* = 0.114 (R1)	0.6105
Homogeneous	21 (49%)	19 (68%)	15 (35%)	17 (61%)	*P* = 0.033 (R2)	
Heterogeneous	22 (51%)	9 (32%)	28 (65%)	11 (39%)		
Calcification					*P* = 0.002 (R1)	0.9481
Present	12 (28%)	0 (0%)	11 (26%)	0 (0%)	*P* = 0.004 (R2)	
Absent	31 (72%)	28 (100%)	32 (74%)	28 (100%)		
Multiple tumors					*P* < 0.001 (R1)	0.8031
Yes	7 (16%)	17 (61%)	5 (12%)	15 (54%)	*P* < 0.001 (R2)	
No	36 (84%)	11 (39%)	38 (88%)	13 (46%)		
Main pancreatic duct dilation					*P* = 0.025 (R1)	
Present	7 (16%)	0 (0%)	10 (23%)	0 (0%)	*P* = 0.006 (R2)	0.8004
Absent	36 (84%)	28 (100%)	33 (77%)	28 (100%)		

PNET pancreatic neuroendocrine tumor, *ccRCC* clear cell renal cell carcinoma, *R1* radiologist 1, *R2* radiologist 2

management differs depending on diagnosis, and prior to definitive therapy, invasive histological sampling is required typically using EUS-FNA-guided biopsy which may be non-diagnostic. Our findings suggest that several subjective and quantitative imaging features at enhanced CT can be used to differentiate PNETs from pancreatic RCC metastases. The presence of tumor calcification and main pancreatic duct dilation were specific features for PNETs, whereas pancreatic RCC metastases tended to be smaller and were more frequently multiple. PNETs appeared subjectively and quantitatively more heterogeneous using texture analysis. Our results suggest that enhanced CT imaging features may accurately differentiate between PNET and pancreatic RCC metastases which may potentially obviate the need for histological sampling in select cases.

Despite the clinical importance, there are limited data available in the literature comparing imaging features between PNETs and pancreatic RCC metastases, which may relate to the challenge of obtaining a sufficient number of patients to perform analyses. Kang et al. compared relative percentage washout using arterial and portal venous phase CT images, and found that the mean washout of pancreatic RCC metastases was greater than that of PNETs [29]. Similar to our study, they also found that pancreatic RCC metastases were more numerous than PNETs; however, unlike our study, they did not observe a significant difference in tumor homogeneity ($P = 0.701$). This may have been due to their inclusion of both arterial phase images, in addition to, portal venous phase images in their qualitative assessment. A limitation of the study by Kang et al. is that they only performed subjective analysis of tumor homogeneity, whereas we performed quantitative texture analysis which has been shown to be more sensitive to differentiate between neoplasms based upon their composition due to the study

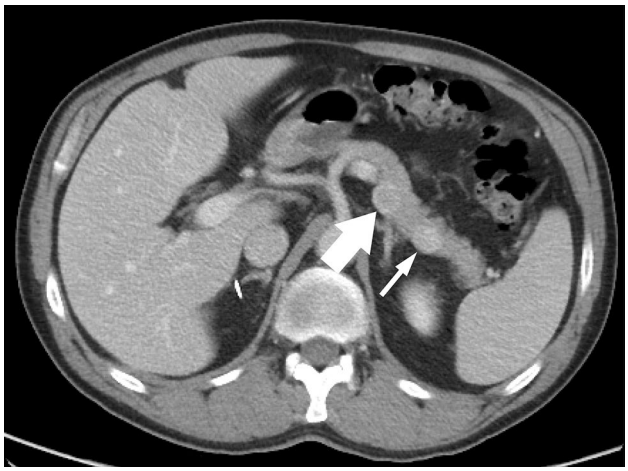

Fig. 3 A 63-year-old female with two pancreatic RCC metastasis. Axial CECT demonstrates two enhancing masses in the pancreas tail (arrows). Pancreatic RCC metastases demonstrated more homogeneous enhancement than PNETs and were more likely to present as multiple pancreatic masses

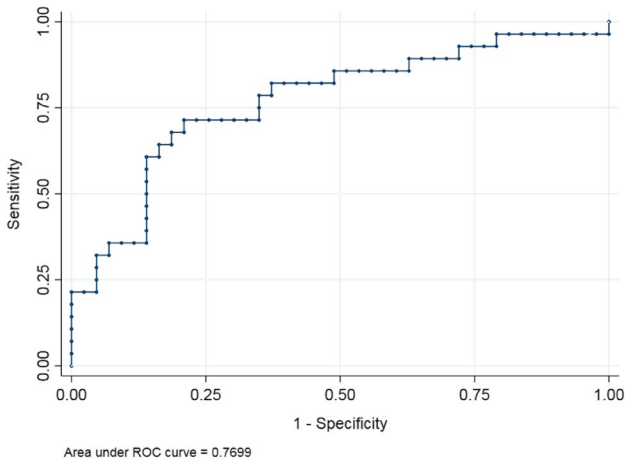

Fig. 4 Receiver operator characteristic curve (ROC) for a logistic regression model combining size and texture features which resulted in an area under the ROC curve of 0.77 (±0.06) with optimal sensitivity and specificity for diagnosis of PNET of 71.4% and 79.1%, respectively

of features at the pixel level which are imperceptible to the human eye [21].

We are unaware any study applying texture analysis to differentiate PNETs and pancreatic RCC metastases on CT or MRI. Qualitative features and texture analysis have, however, been shown to be helpful for determining PNET grade using CT. For example, Canellas et al. found that tumor size larger than 2 cm, vascular involvement, MPD dilation, and lymphadenopathy, and the texture feature entropy were all associated with higher grade (grade 2 and 3) disease [23]. Similarly, Choi et al. found that an ill-defined margin and texture features of lower sphericity, higher skewness, and lower kurtosis were associated with grade 2 and 3 PNETs [30]. Even though our PNET cohort consisted of mainly low-grade tumors, we demonstrated that PNETs overall were more heterogeneous both subjectively and quantitatively compared to pancreatic RCC metastases.

A recent study by Lyu et al. demonstrated that the presence of intratumoral lipid using chemical shift MRI may be useful to differentiate PNETs from pancreatic RCC

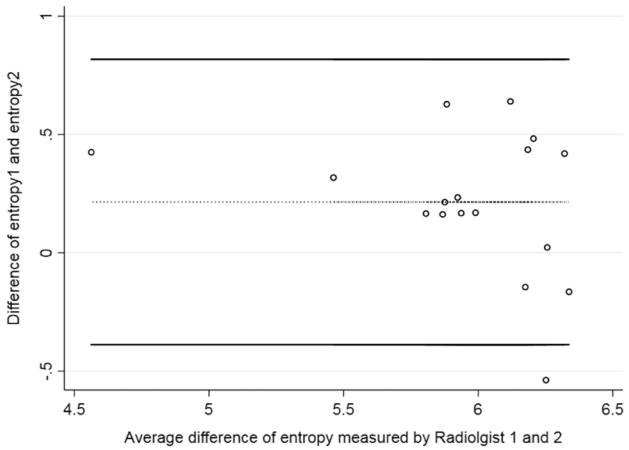

Fig. 5 Bland–Altman plot for reproducibility of texture analysis measurements, which was substantial with a low mean difference of 0.21 ± 0.30

Table 2 Comparison of quantitative variables of pancreatic neuroendocrine tumors and pancreatic renal cell carcinoma metastases at enhanced CT

Feature	PNET	Pancreatic RCC metastases	*P* value[a]
Size (mm)	37 ± 23 (10–96)	26 ± 21 (9–95)	0.038
Mean (HU)	108.4 ± 39.4 (42.6–200.3)	108.7 ± 33.5 (53.5–191.1)	0.969
Median (HU)	108.7 ± 36.2 (33.0–199.1)	109.9 ± 35.1 (50.0–196.1)	0.895
Kurtosis	1.49 ± 6.56 (−0.68 to 34.55)	0.51 ± 1.07 (−1.12 to 4.30)	0.067
Skewness	0.13 ± 0.96 (−0.79 to 4.47)	−0.21 ± 0.54 (−1.47 to 0.59)	0.099
Entropy	6.32 ± 0.49 (5.36–7.45)	5.96 ± 0.53 (4.34–7.34)	0.004

HU Hounsfield units, *PNET* pancreatic neuroendocrine tumor, *RCC* renal cell carcinoma

[a]Comparisons were performed using multivariable logistic regression

metastases, since it is known that RCC metastases from clear cell RCC may contain intratumoral lipid [31], whereas the presence of intratumoral lipid should not be present in PNETs. Clear cell RCC metastases do not always appear similar on imaging to the primary tumor from which they spread. Moosavi et al. found that in 20% of RCC metastases which contained intracellular lipid at chemical shift MRI, the finding was not present in the primary tumor [32]. Further complicating recognition of RCC metastases is the sometimes-long duration between initial RCC presentation and the development of metastases, which can be 12 or more years, and also that the pancreas can be the sole site of recurrence [7, 8]. Given the ubiquity of incidentally discovered renal masses detected on CT or MRI in clinical practice which can occur in up to 40% of patients [33], we believe it useful to establish features on imaging that can be used to differentiate PNETs and RCCs.

PNETs often appear as solid hypervascular neoplasms on arterial or occasionally portal venous phase imaging [34]. Prior work suggests that approximately 22% of PNETs contain calcification [35], similar to our study. Although MPD dilation is more commonly seen secondary to pancreatic adenocarcinoma rather than PNETs, a minority of PNETs have been found to cause MPD dilation, which may be due to mass effect from the tumor itself or from fibrotic stricture formation secondary to serotonin or related metabolites released by the tumor [36]. In our study, we found that up to one-quarter of PNETs had associated MPD dilation, whereas this finding was not present for any pancreatic RCC metastases.

Molecular imaging techniques such as Gallium 68 DOTATATE PET/CT or octreotide scintigraphy can be used to detect neuroendocrine tumors. While generally accurate, these techniques depend on neuroendocrine tumor somatostatin receptor expression which is not always high (particularly in poorly differentiated subtypes) and have several other pitfalls [37]. Furthermore, some RCCs express somatostatin receptors and can demonstrate uptake [38]. We consider molecular imaging techniques complementary to enhanced CT at present, which has higher spatial resolution and provides good anatomic detail.

A limitation of our study includes the relatively small sample size, which we attempted to overcome by our multi-institutional study design. Future larger scale studies are required to validate our results if imaging is to replace histological sampling to differentiate pancreatic RCC metastases from PNETs. We studied portal venous phase enhanced CT images, rather than unenhanced or arterial phase enhanced CT images, primarily since these were most frequently available in our cohort to maximize our sample size. Analysis of additional phases may provide further information and improve accuracy which may be an area for future research. Nevertheless, we believe that our results which demonstrate a difference between PNET and RCC metastases at portal venous phase enhanced CT strengthens our study since portal venous phase imaging is most frequently performed in clinical practice, particularly among incidentally discovered pancreatic masses. We did not perform a secondary analysis comparing PNETs by grade to RCC metastases given the relatively small number of high-grade PNETs in our cohort. Lastly, we included only cases with surgical confirmation rather than EUS-FNA biopsy specimens to ensure accurate final diagnosis as EUS-FNA can sometimes lead to an incorrect diagnosis or not provide a specific diagnosis due to undersampling [15]. Excluding diagnoses obtained with FNA biopsies reduced our total number of cases.

In conclusion, our study demonstrates that subjective imaging features and quantitative texture analysis may differentiate PNET from pancreatic RCC metastases. Tumor calcification, solitary masses, and MPD dilation were specific features for PNET but lacked sensitivity, whereas the quantitative texture analysis feature entropy improved sensitivity for diagnosis with moderate overall accuracy. Our results suggest that imaging features at enhanced CT may accurately differentiate between pancreatic RCC metastases and PNET and could potentially obviate the need for histological confirmation, especially to confirm the presence of metastatic disease in patients with a history of RCC, although will require confirmation in larger sample sizes.

Acknowledgements All authors have no grants, disclosures, or other assistance to acknowledge.

Compliance with ethical standards

Conflict of interest The authors have no conflicts of interest to declare.

Ethical approval All procedures performed in studies involving human participants were in accordance with the ethical standards of the institutional and/or national research committee and with the 1964 Helsinki declaration and its later amendments or comparable ethical standards.

Informed consent This retrospective image review study was approved by the institution review boards with a waiver of informed consent for retrospective image analysis.

References

1. Masetti M, Zanini N, Martuzzi F, et al. (2010) Analysis of prognostic factors in metastatic tumors of the pancreas: a single-center experience and review of the literature. Pancreas 39:135-143
2. Brufau BP, Cerqueda CS, Villalba LB, et al. (2013) Metastatic renal cell carcinoma: radiologic findings and assessment of response to targeted antiangiogenic therapy by using multidetector CT. Radiographics 33:1691-1716
3. Adsay NV, Andea A, Basturk O, et al. (2004) Secondary tumors of the pancreas: an analysis of a surgical and autopsy database and review of the literature. Virchows Arch 444:527-535

4. Sheth S, Hruban RK, Fishman EK (2002) Helical CT of islet cell tumors of the pancreas: typical and atypical manifestations. AJR Am J Roentgenol 179:725-730
5. Taouli B, Ghouadni M, Correas JM, et al. (2003) Spectrum of abdominal imaging findings in von Hippel-Lindau disease. AJR Am J Roentgenol 181:1049-1054
6. Chrom P, Stec R, Bodnar L, Szczylik C (2018) Prognostic Significance of Pancreatic Metastases from Renal Cell Carcinoma in Patients Treated with Tyrosine Kinase Inhibitors. Anticancer Res 38:359-365
7. Kassabian A, Stein J, Jabbour N, et al. (2000) Renal cell carcinoma metastatic to the pancreas: a single-institution series and review of the literature. Urology 56:211-215
8. Sellner F, Tykalsky N, De Santis M, Pont J, Klimpfinger M (2006) Solitary and multiple isolated metastases of clear cell renal carcinoma to the pancreas: an indication for pancreatic surgery. Ann Surg Oncol 13:75-85
9. Kazanjian KK, Reber HA, Hines OJ (2006) Resection of pancreatic neuroendocrine tumors: results of 70 cases. Arch Surg 141:765-769; discussion 769-770
10. Lee LC, Grant CS, Salomao DR, et al. (2012) Small, nonfunctioning, asymptomatic pancreatic neuroendocrine tumors (PNETs): role for nonoperative management. Surgery 152:965-974
11. Rosenberg AM, Friedmann P, Del Rivero J, Libutti SK, Laird AM (2016) Resection versus expectant management of small incidentally discovered nonfunctional pancreatic neuroendocrine tumors. Surgery 159:302-309
12. Raymond E, Dahan L, Raoul JL, et al. (2011) Sunitinib malate for the treatment of pancreatic neuroendocrine tumors. N Engl J Med 364:501-513
13. Dutcher JP (2013) Recent developments in the treatment of renal cell carcinoma. Ther Adv Urol 5:338-353
14. Sperti C, Moletta L, Patane G (2014) Metastatic tumors to the pancreas: the role of surgery. World J Gastrointest Oncol 6:381-392
15. Bernstein J, Ustun B, Alomari A, et al. (2013) Performance of endoscopic ultrasound-guided fine needle aspiration in diagnosing pancreatic neuroendocrine tumors. Cytojournal 10:10
16. Ardengh JC, Lopes CV, Kemp R, et al. (2013) Accuracy of endoscopic ultrasound-guided fine-needle aspiration in the suspicion of pancreatic metastases. BMC Gastroenterol 13:63
17. Pannala R, Hallberg-Wallace KM, Smith AL, et al. (2016) Endoscopic ultrasound-guided fine needle aspiration cytology of metastatic renal cell carcinoma to the pancreas: A multi-center experience. Cytojournal 13:24
18. Hodgdon T, McInnes MD, Schieda N, et al. (2015) Can Quantitative CT Texture Analysis be Used to Differentiate Fat-poor Renal Angiomyolipoma from Renal Cell Carcinoma on Unenhanced CT Images? Radiology 276:787-796
19. Eilaghi A, Baig S, Zhang Y, et al. (2017) CT texture features are associated with overall survival in pancreatic ductal adenocarcinoma - a quantitative analysis. BMC Med Imaging 17:38
20. Smith AD, Gray MR, del Campo SM, et al. (2015) Predicting Overall Survival in Patients With Metastatic Melanoma on Antiangiogenic Therapy and RECIST Stable Disease on Initial Posttherapy Images Using CT Texture Analysis. AJR Am J Roentgenol 205:W283-293
21. Schieda N, Thornhill RE, Al-Subhi M, et al. (2015) Diagnosis of Sarcomatoid Renal Cell Carcinoma With CT: Evaluation by Qualitative Imaging Features and Texture Analysis. AJR Am J Roentgenol 204:1013-1023
22. Schieda N, Lim RS, Krishna S, et al. (2018) Diagnostic Accuracy of Unenhanced CT Analysis to Differentiate Low-Grade From High-Grade Chromophobe Renal Cell Carcinoma. AJR Am J Roentgenol 210:1079-1087
23. Canellas R, Burk KS, Parakh A, Sahani DV (2018) Prediction of Pancreatic Neuroendocrine Tumor Grade Based on CT Features and Texture Analysis. AJR Am J Roentgenol 210:341-346
24. Ronkainen H, Soini Y, Vaarala MH, Kauppila S, Hirvikoski P (2010) Evaluation of neuroendocrine markers in renal cell carcinoma. Diagn Pathol 5:28
25. Tacha D, Qi W, Zhou D, Bremer R, Cheng L (2013) PAX8 mouse monoclonal antibody [BC12] recognizes a restricted epitope and is highly sensitive in renal cell and ovarian cancers but does not cross-react with b cells and tumors of pancreatic origin. Appl Immunohistochem Mol Morphol 21:59-63
26. Zhang GM, Sun H, Shi B, Jin ZY, Xue HD (2017) Quantitative CT texture analysis for evaluating histologic grade of urothelial carcinoma. Abdom Radiol (NY) 42:561-568
27. Mammen S, Krishna S, Quon M, et al. (2018) Diagnostic Accuracy of Qualitative and Quantitative Computed Tomography Analysis for Diagnosis of Pathological Grade and Stage in Upper Tract Urothelial Cell Carcinoma. J Comput Assist Tomogr 42:204-210
28. Rasband W (1997-2016) ImageJ, U. S. National Institutes of Health, Bethesda, Maryland, USA. https://imagej.nih.gov/ij/. Accessed September 1, 2018.
29. Kang TW, Kim SH, Lee J, et al. (2015) Differentiation between pancreatic metastases from renal cell carcinoma and hypervascular neuroendocrine tumour: Use of relative percentage washout value and its clinical implication. Eur J Radiol 84:2089-2096
30. Choi TW, Kim JH, Yu MH, Park SJ, Han JK (2018) Pancreatic neuroendocrine tumor: prediction of the tumor grade using CT findings and computerized texture analysis. Acta Radiol 59:383-392
31. Lyu HL, Cao JX, Wang HY et al (2018) Differentiation between pancreatic metastases from clear cell renal cell carcinoma and pancreatic neuroendocrine tumor using double-echo chemical shift imaging. Abdom Radiol (NY). https://doi.org/10.1007/s00261-018-1539-7
32. Moosavi B, Shabana WM, El-Khodary M, et al. (2016) Intracellular lipid in clear cell renal cell carcinoma tumor thrombus and metastases detected by chemical shift (in and opposed phase) MRI: radiologic-pathologic correlation. Acta Radiol 57:241-248
33. Carrim ZI, Murchison JT (2003) The prevalence of simple renal and hepatic cysts detected by spiral computed tomography. Clin Radiol 58:626-629
34. Fidler JL, Fletcher JG, Reading CC, et al. (2003) Preoperative detection of pancreatic insulinomas on multiphasic helical CT. AJR Am J Roentgenol 181:775-780
35. Eelkema EA, Stephens DH, Ward EM, Sheedy PF 2nd (1984) CT features of nonfunctioning islet cell carcinoma. AJR Am J Roentgenol 143:943-948
36. Kawamoto S, Shi C, Hruban RH, et al. (2011) Small serotonin-producing neuroendocrine tumor of the pancreas associated with pancreatic duct obstruction. AJR Am J Roentgenol 197:W482-488
37. Hofman MS, Lau WF, Hicks RJ (2015) Somatostatin receptor imaging with 68 Ga DOTATATE PET/CT: clinical utility, normal patterns, pearls, and pitfalls in interpretation. Radiographics 35:500-516
38. Freudenberg LS, Gauler T, Gorges R, et al. (2008) Somatostatin receptor scintigraphy in advanced renal cell carcinoma. Results of a phase II-trial of somatostatine analogue therapy in patients with advanced RCC. Nuklearmedizin 47:127-131